Inter-Leaflet Interaction and Asymmetry in Phase Separated Lipid Bilayers: Molecular Dynamics Simulations

Jason D. Perlmutter[1], Jonathan N. Sachs*[1]

[1]*Biomedical Engineering, University of Minnesota, Minneapolis, Minnesota 55455, USA*

Supplemental Methods

For each of the asymmetric and symmetric bilayers at a 2:2:1 ratio, three distinct starting configurations were used. In each case, two of the starting configurations were composed of a randomized lateral distribution. The third set of simulations used a starting configuration intended to be far from the previously observed local equilibria. For the symmetric bilayers, starting configurations were adapted from a completed simulation with the opposite registration behavior, i.e. a bilayer which had in previous simulations formed registered domains was started in an anti-registered conformation, and vice-versa. For the asymmetric bilayers, a far from equilibrium initial configuration was formed by taking a simulated asymmetric bilayer, and switching the location of the saturated and unsaturated lipid in the ternary leaflet, leaving all the cholesterol co-localized with the unsaturated lipid. In the asymmetric bilayer containing di-6:0 this resulted in the formation of a gel phase and instead an additional random configuration was used. For the single-component di-4:2 simulation, we have used 3 different starting velocities. In each case, the qualitative results, including phase separation and registration vs. anti-registration, are the same for each starting configuration. Additionally, the quantitative results from the separate simulations are indistinguishable, as demonstrated by the very small amount of variation presented in Table 2. The convergence of multiple starting configurations to the same local equilibrium suggests that we have reached the most favorable conformation, given our restriction of phospholipid flip-flop.

Supplemental Figures

S1 – Six simulations composed of different amounts of di-4:2 were first conducted in order to determine the lateral area. The bottom panel shows the box length (filled diamonds) and average area per lipid (clear boxes).

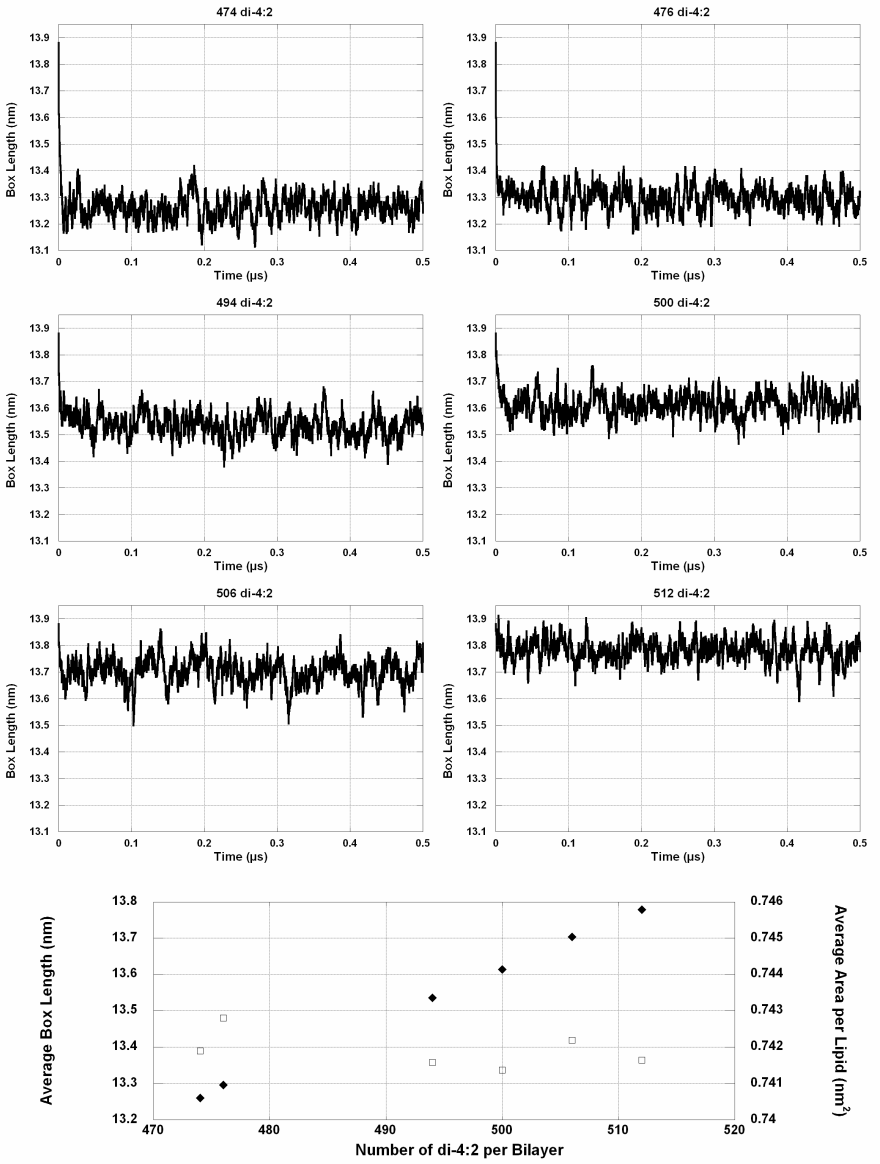

S2 - Timeseries showing equilibration for each of the bilayers on the μs timescale. Box length (black line) and size of the disordered domain (top leaflet = black line, clear squares; bottom leaflet = gray line, filled circles).

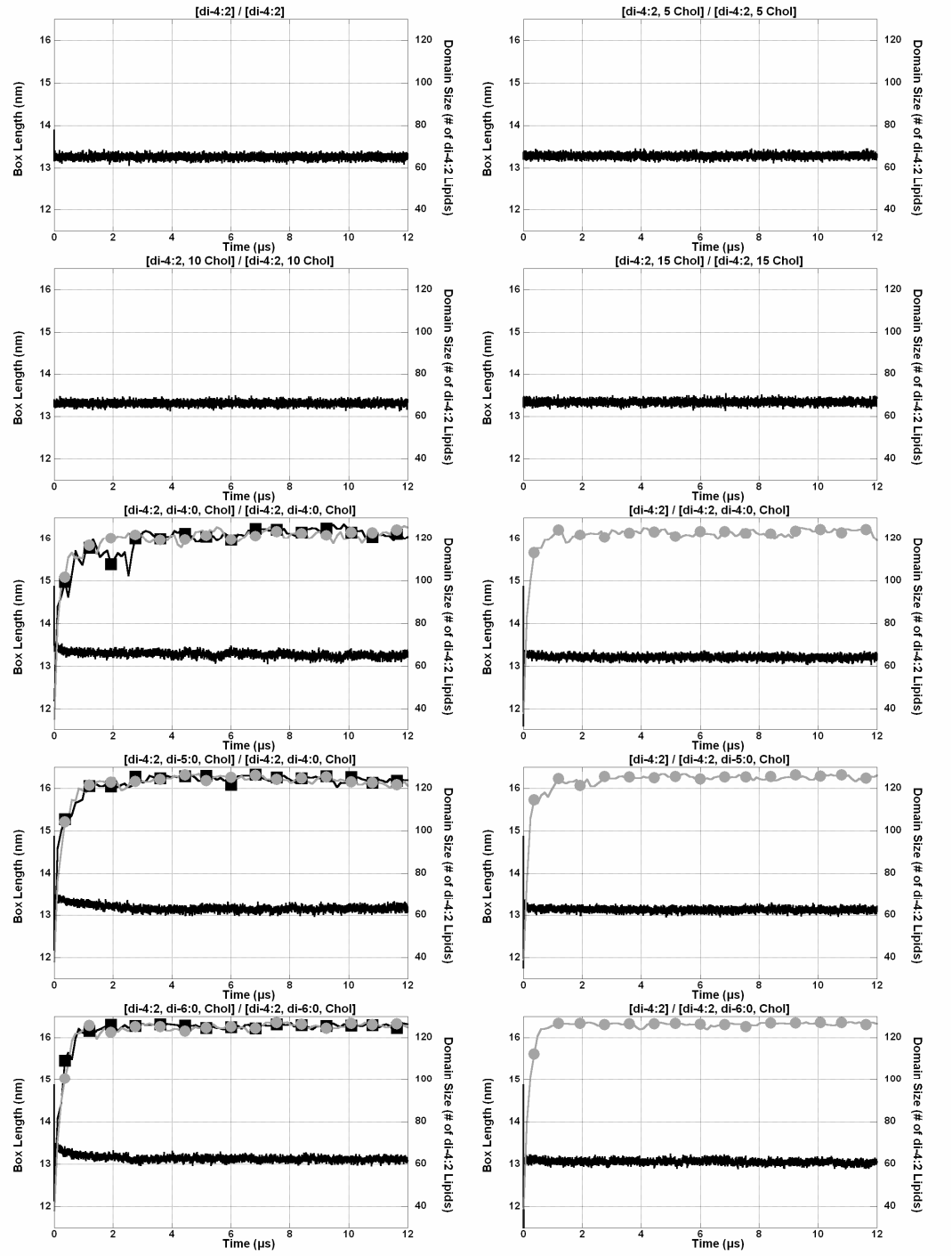

S3 – Equilibration of the inter-leaflet effects. Top Panel: The tilt in the region opposite the ordered domain in the [di-4:2] / [di-4:2, di-4:0, Chol] bilayer (black) as a function of simulation time, compared with the average of the single component [di-4:2] / [di-4:2] bilayer (dotted black line) and [di-4:2, 15 Chol] / [di-4:2, 15 Chol] (dotted gray line). Middle Panel: The RMSD of the distance of the lipid headgroups from an average flat surface, reflecting the development of curvature (as well as dynamic motion). The RMSD for the top leaflets of the [di-4:2] / [di-4:2] (Black line), [di-4:2] / [di-4:2, di-4:0, Chol] (Gray line), [di-4:2] / [di-4:2, di-5:0, Chol] (Gray Circles), [di-4:2] / [di-4:2, di-6:0, Chol] (Triangles). Bottom Panel: Lateral diffusion as a function of simulation time, in the top leaflet of the [di-4:2] / [di-4:2, di-4:0, Chol] bilayer.

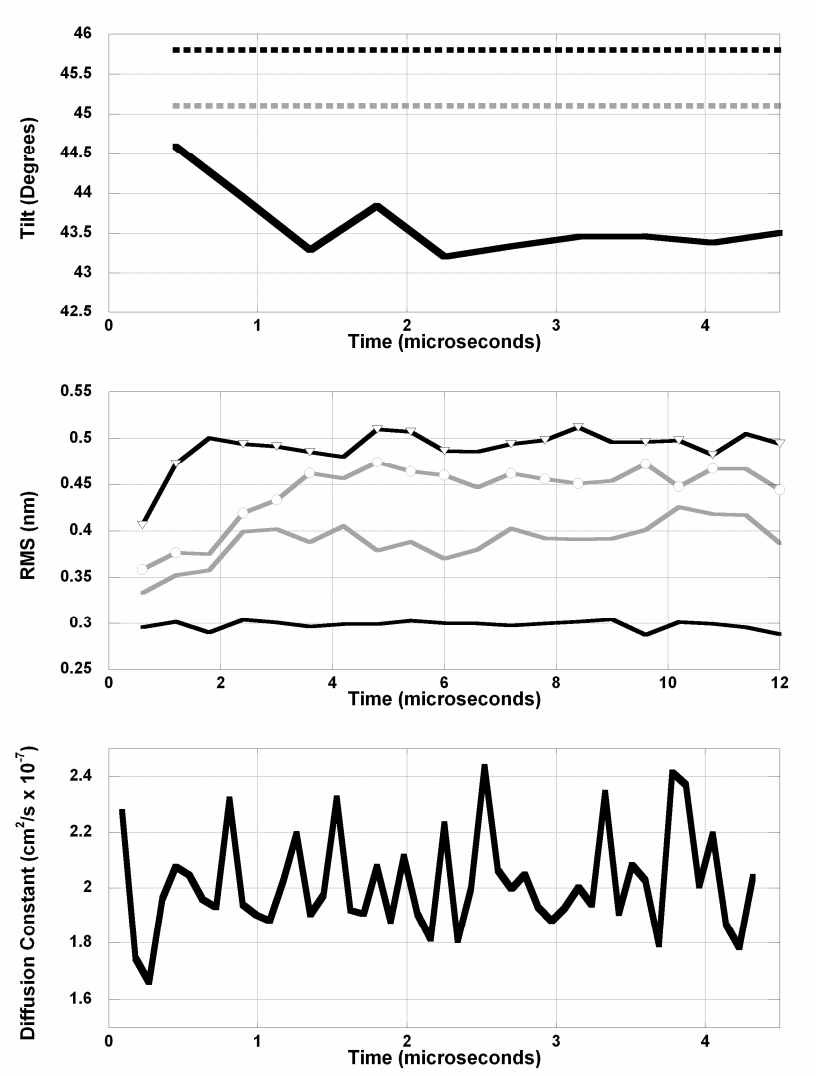

S4 – Timeseries showing equilibration of the cholesterol distribution on the μs timescale. In both the symmetric [di-4:2, di-4:0, Chol] / [di-4:2, di-4:0, Chol] (top) and asymmetric [di-4:2] / [di-4:2, di-4:0, Chol] (middle) bilayers, the inter-leaflet cholesterol distribution equilibrates rapidly (<200ns). Cholesterols are assigned to a leaflet as described in the Methods section, except with the addition of identifying those cholesterols which are mid-flip-flop. Cholesterols are categorized as mid-flip-flop if their hydroxyl groups are in between the top acyl chain groups of the nearest lipids in both the top and bottom leaflets.

The bottom panel presents an additional test of the rate of equilibration. The cholesterol in the top leaflet of the symmetric [di-4:2, di-4:0, Chol] / [di-4:2, di-4:0, Chol] bilayer was removed, leaving only the cholesterol in the bottom leaflet. In less than 2 μs of simulation, the cholesterol reaches an equal distribution of cholesterol between the two leaflets. This demonstrates that even in a starting configuration far from equilibrium, the cholesterol distribution equilibrates within < 2 μs.

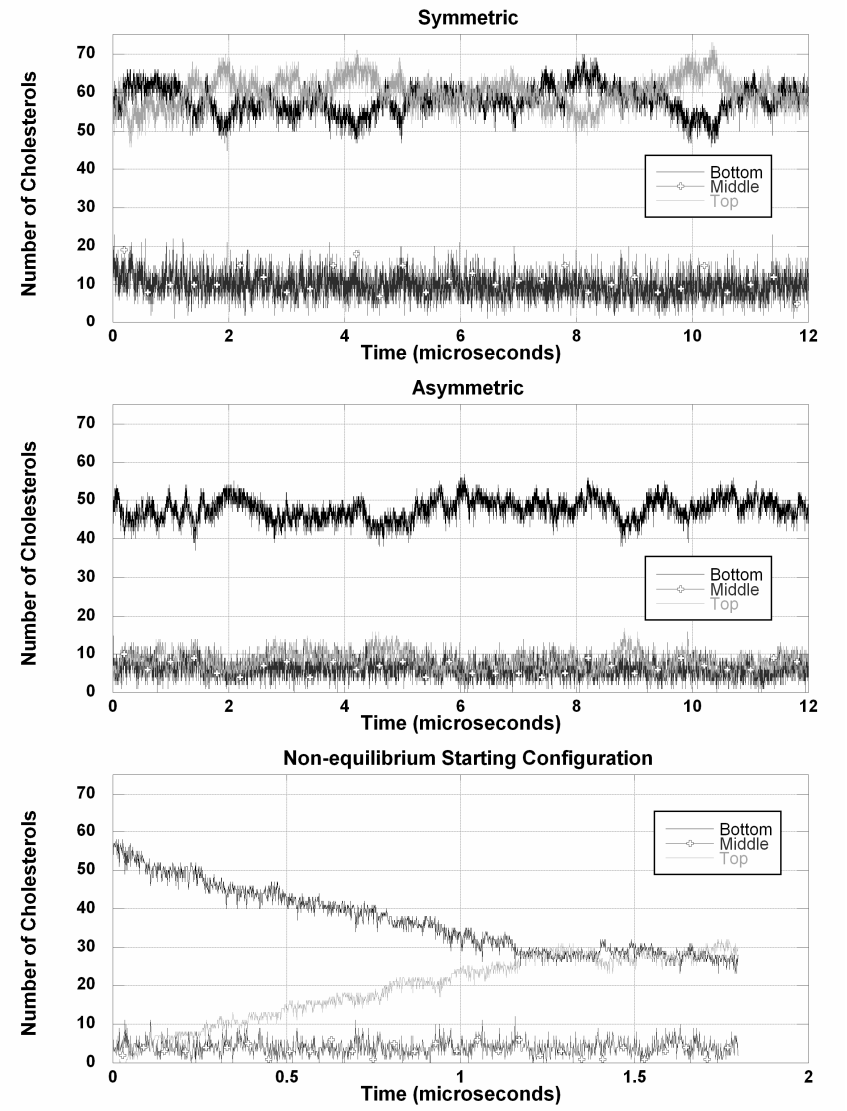

S5 - The effect of cholesterol on per-leaflet component distributions (di-unsaturated lipid and cholesterol), surface curvature, and tilt angles. The effect of cholesterol on lipid tilt is less than observed in the asymmetric bilayers (Figures 2 and 7), demonstrating that cholesterol is not the cause of the reduction in tilt angles in the asymmetric bilayers.

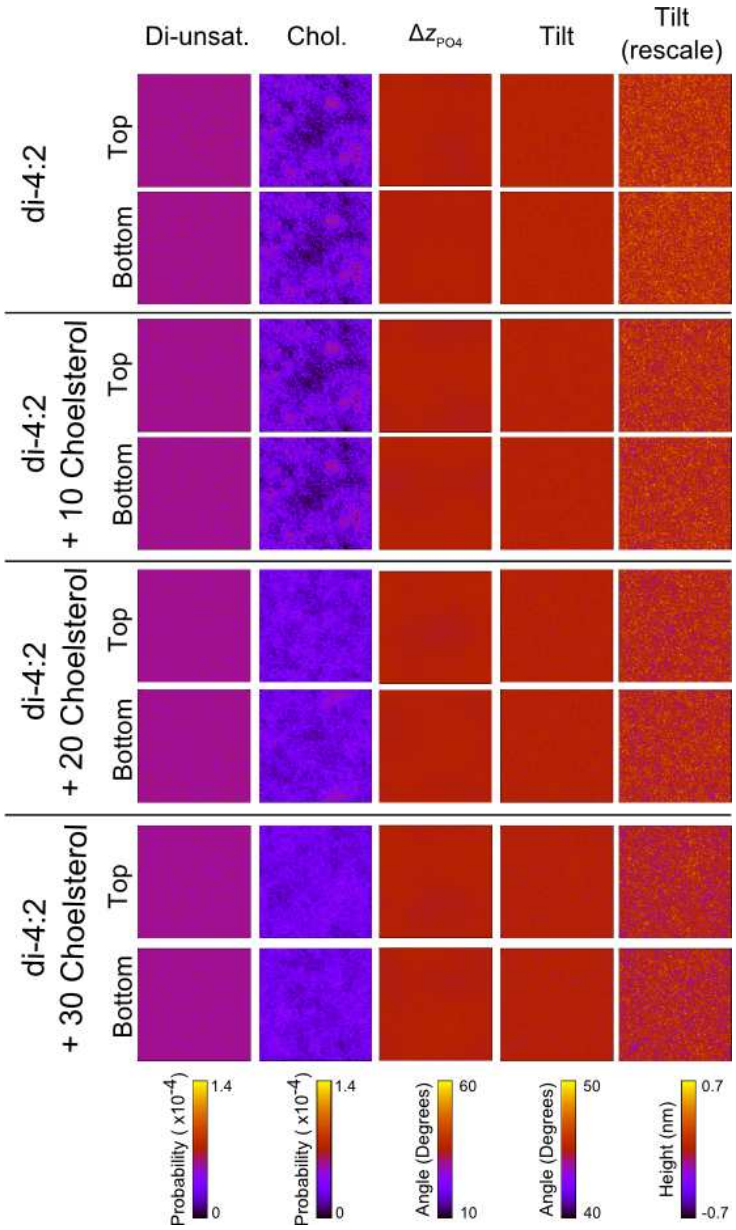

S6 - The effect of phase asymmetry on lipid tilt angles (Top); rotational autocorrelation (Middle); and lateral mean squared displacement (Bottom). Data is for di-4:2 from either the top leaflet of [di-4:2] / [di-4:2] (black line), [di-4:2, di-4:0, Chol] / [di-4:2, di-4:0, Chol] (diamonds), or [di-4:2] / [di-4:2, di-4:0, Chol] (gray line).

Each panel suggests that when considering the average of all the di-4:2 lipids in the leaflet, the magnitude of the intra-leaflet ordering effect is greater than the inter-leaflet ordering effect. In the top panel, the distribution of tilt angles is shifted to the left in the top leaflet of the asymmetric bilayer by an inter-leaflet effect, but the distribution is shifted further by an intra-leaflet effect in the symmetric, ternary bilayer. A similar pattern is observed for the rotational freedom in the middle panel and the lateral diffusion in bottom panel, where the inter-leaflet effect is particularly slight. In each case, though the di-4:2 lipid behaviour may change due to environment, it is still consistently less ordered than the di-4:0 lipids (not shown).

Calculation of the lateral diffusion rates allows comparison with experiment. The relative reduction observed due to the intra-leaflet effect is in agreement with previous simulations[1] as well as experiment[2-4]. In terms of the absolute values, these experiments on phase separated, phase-symmetric bilayers have shown a wide range of results, with values for L_o domains ranging from 0.01 – 10 x 10^{-7} cm^2/s, and 0.5 – 100 x 10^{-7} cm^2/s for L_d domains[3, 4].

Considering the inter-leaflet effect, the diffusion of the di-unsaturated lipid in the single-component leaflet of the asymmetric [di-4:2]/[di-4:2, di-4:0, Chol] bilayer (D = 1.94 x 10^{-7} cm^2/s) is slightly less than the single component [di-4:2]/[di-4:2] case. This is similar to recent experimental results which showed a negligible inter-leaflet effect on the lateral diffusion in similar systems[2, 5].

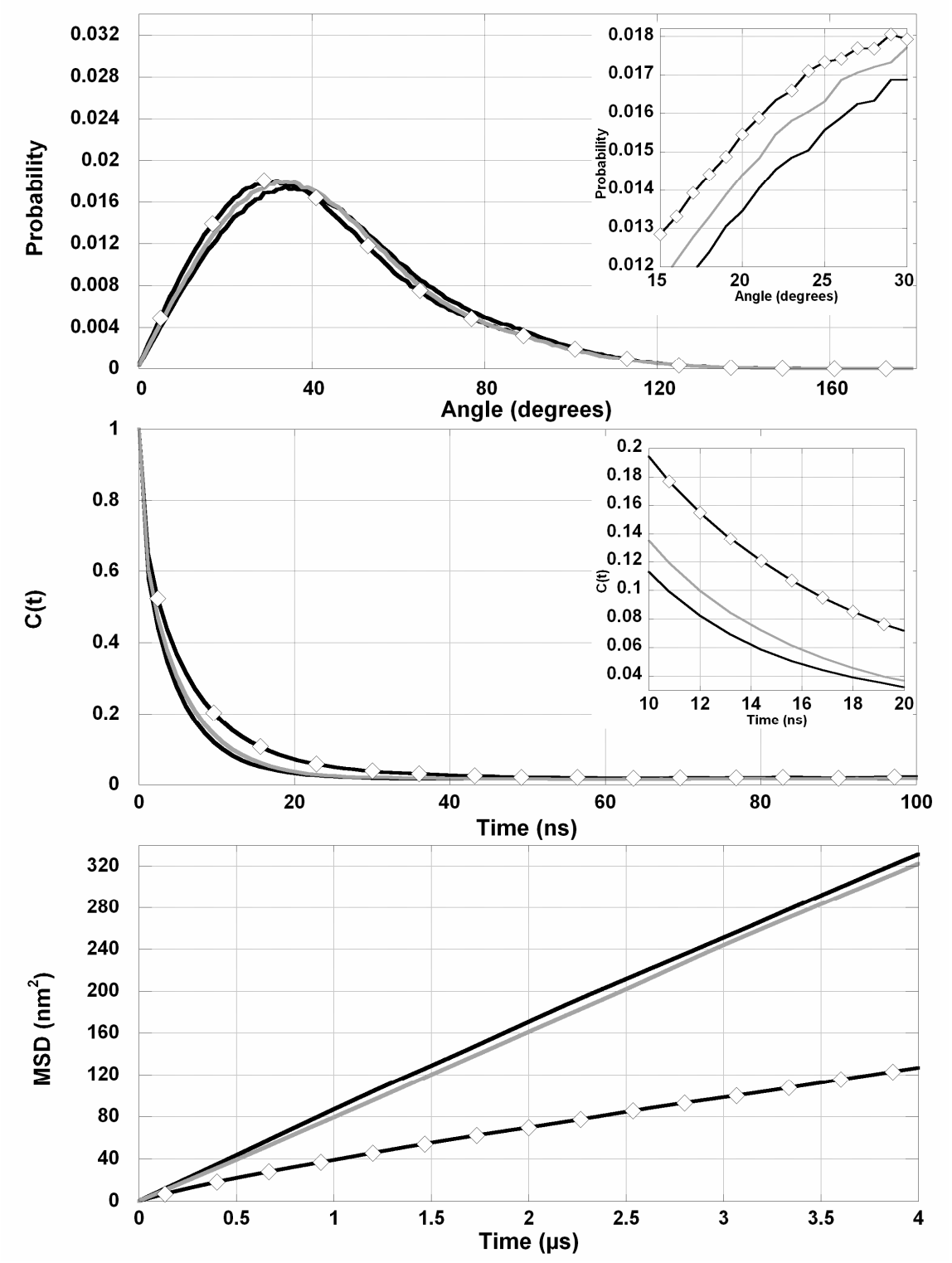
Probability
Angle (degrees)
C(t)
Time (ns)
MSD (nm^2)
Time (μs)

S7 – The inter- and intra-leaflet effects on lipid tilt, for the [di-4:2] / [di-4:2] , [di-4:2, di-4:0, Chol] / [di-4:2, di-4:0, Chol], [di-4:2] / [di-4:2, di-4:0, Chol], [di-4:2] / [di-4:2, di-5:0, Chol], and [di-4:2] / [di-4:2, di-6:0, Chol] bilayers. The lipid tilt is reduced in the ternary leaflets by an intra-leaflet effect and in the top leaflet of the asymmetric bilayers by an inter-leaflet effect. Solid Gray = di-unsaturated lipid density in the lower leaflet, Solid Black = saturated lipid density in the lower leaflet, Circles = lipid tilt in top leaflet, Triangles = lipid tilt in bottom leaflet.

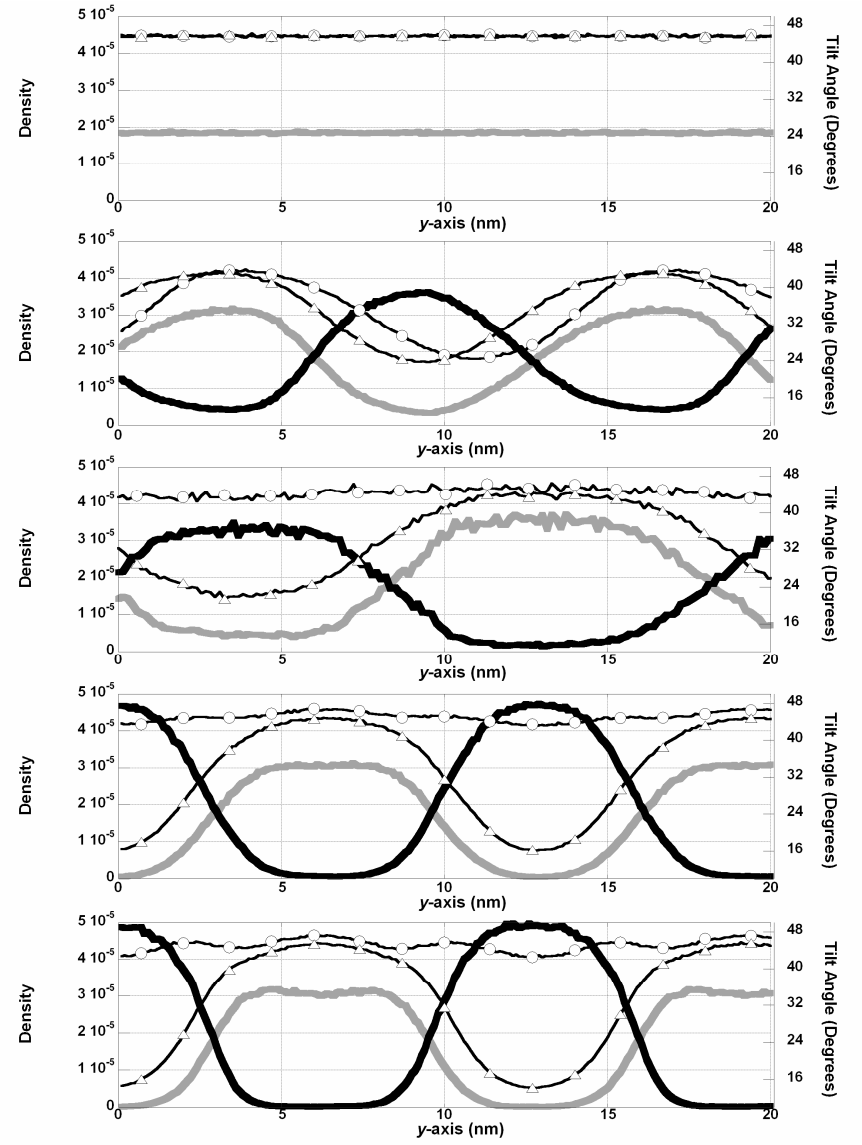

S8 – The order parameter of di-4:2 in the top leaflet of the compositionally symmetric, anti-registered [di-4:2, di-6:0, Chol] / [di-4:2, di-6:0, Chol] bilayer (black) and bottom leaflet of the [di-4:2] / [di-4:2, di-6:0, Chol] bilayer (gray). Both show ordering around the L_o domain (centered at x=0 nm) and the anti-registered bilayer also shows an inter-leaflet ordering effect at x~6.5.

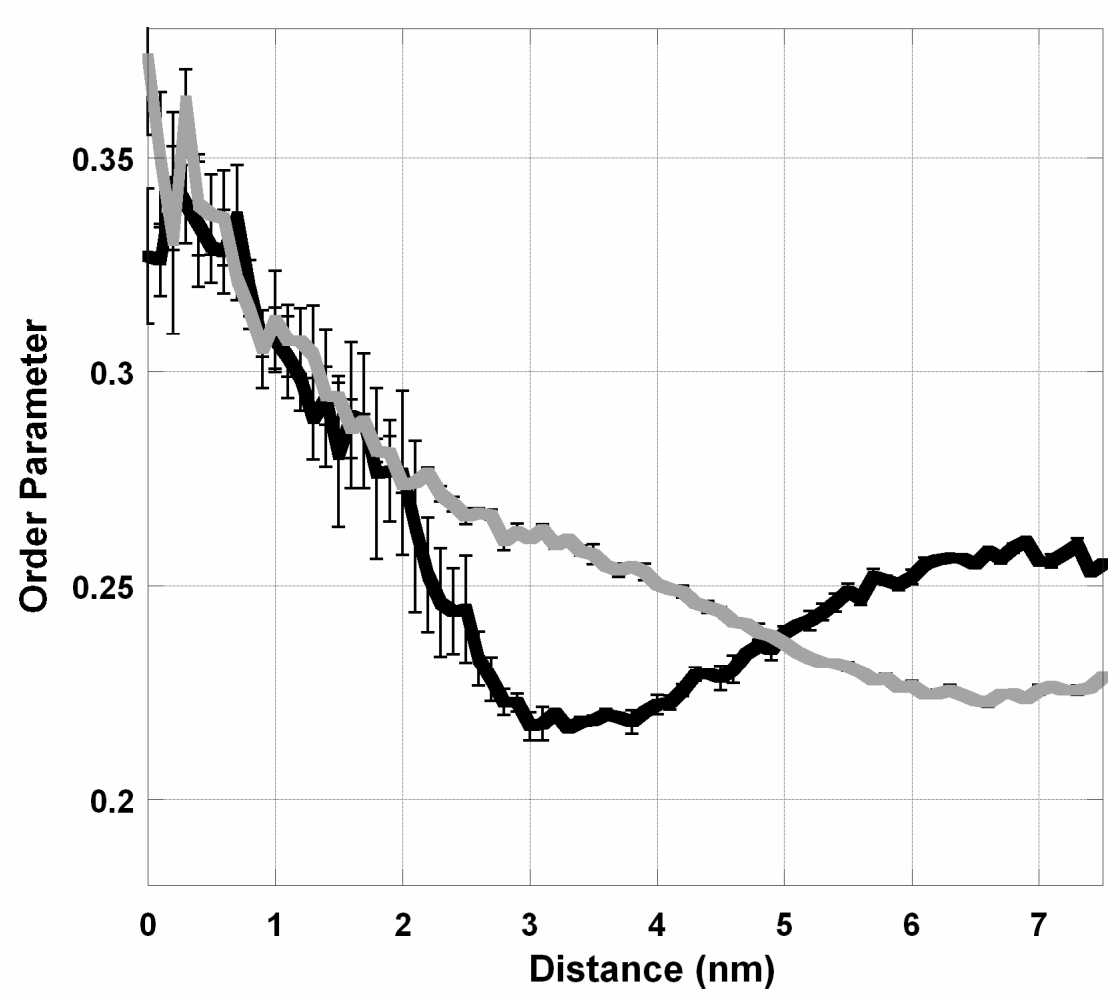

S9 – The height of the surfaces composed either of the top leaflet phosphate or terminal tail groups (gray) and bottom leaflet phosphate or terminal tail groups (black). 2-D data was averaged in the *x*-axis, except for the [di-4:2] / [di-4:2, di-4:0, Chol] bilayer which is averaged along the diagonal (*x*=*y*). Note that the axes are scaled differently.

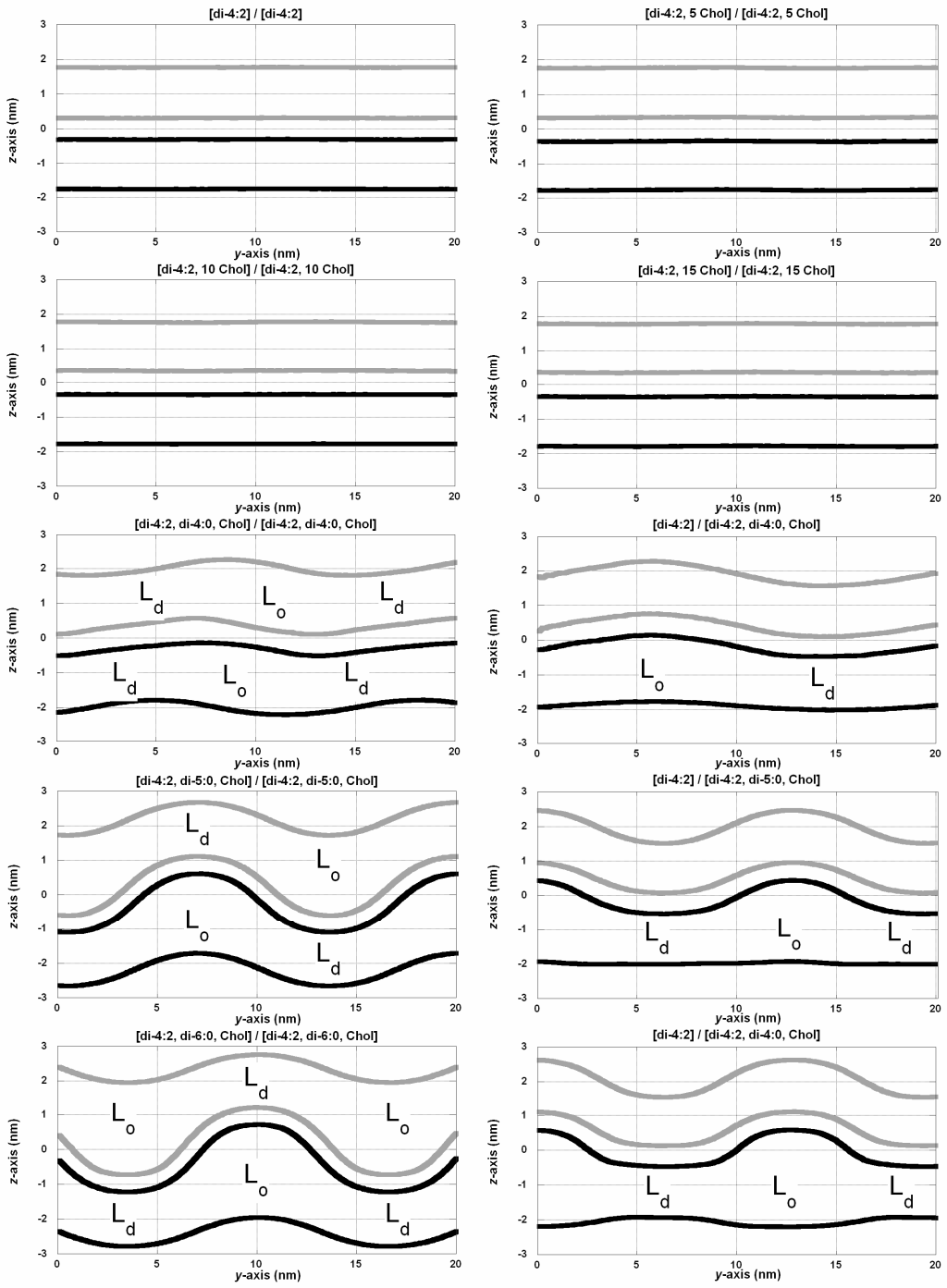

S10 – The effect of molar ratios on anti-registered bilayer structure. Compared to the 2:2:1 mixture (top), the system with less saturated lipid (4:2:1, middle) shows a similar (and perhaps slightly larger) degree of curvature. The system with more saturated lipid (1:2:1, bottom) shows less curvature. The 4:2:1 data comes from an averaging along the X-axis in the left-most side of figure 6, over a range of 1 nm.

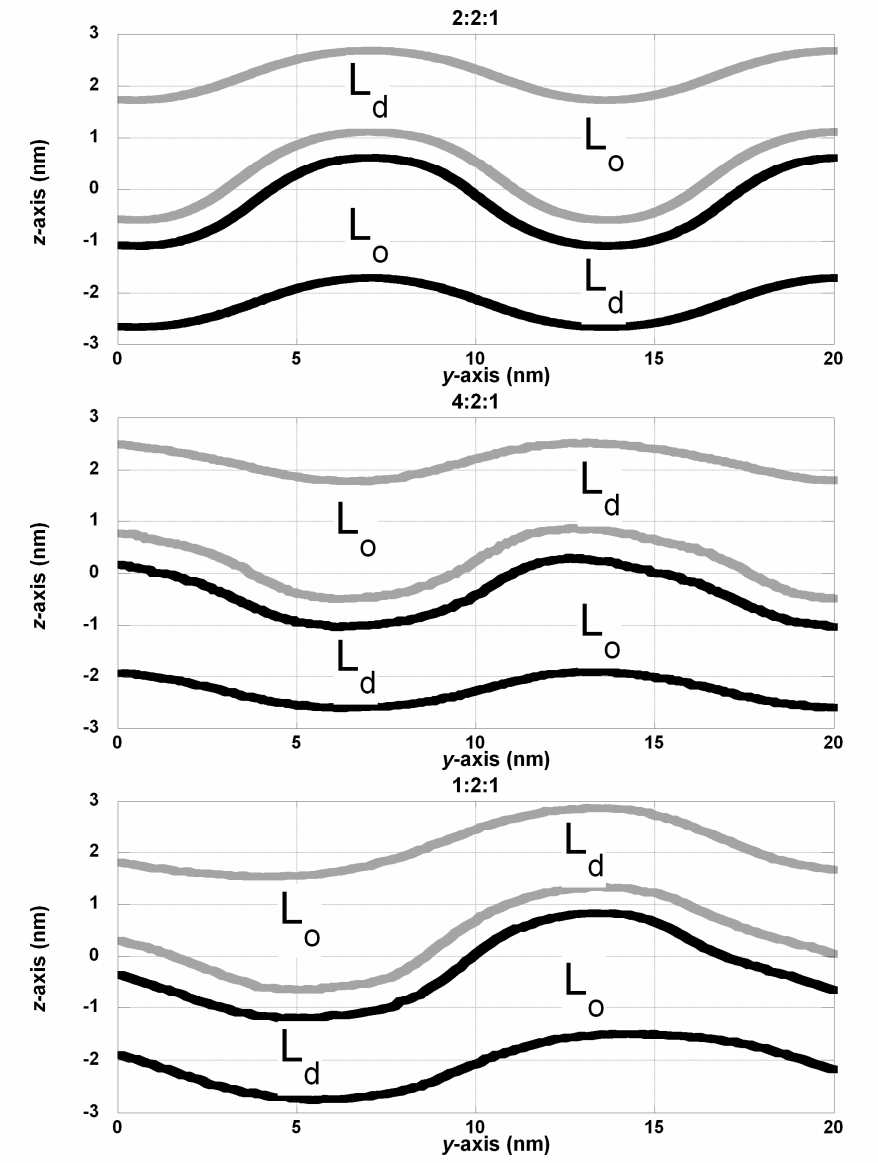

S11 – One possible cause of the curvature observed in the asymmetric simulations is unequal areas in the two leaflets. Though we have been careful to avoid area mismatch, by first simulating compositionally symmetric bilayers, it still possible that area mismatch exists, either due to an inter-leaflet perturbation or the flip-flop of cholesterol. However, Figure S2 shows that in the control simulations the effect of these cholesterols on the area is low; 10 cholesterols increase the area of a leaflet of 237 di-4:2 by 1.3 nm^2, or a <1% increase.

In order to ensure that area mismatch is not the origin of the curvature we observe, we present an additional control simulation, in which the [di-4:2]/[di-4:2, di-4:0, Chol] bilayer is re-simulated with 10 less di-4:2 lipids in the top leaflet. This reduction in area in the top leaflet should over-compensate for the flip-flop of 10 cholesterol into the top leaflet. This change in area has a minimal effect on the curvature, further suggesting that the curvature is not primarily caused by an area mismatch. Note that this data is the average of 2-dimensional data in the *x*-axis.

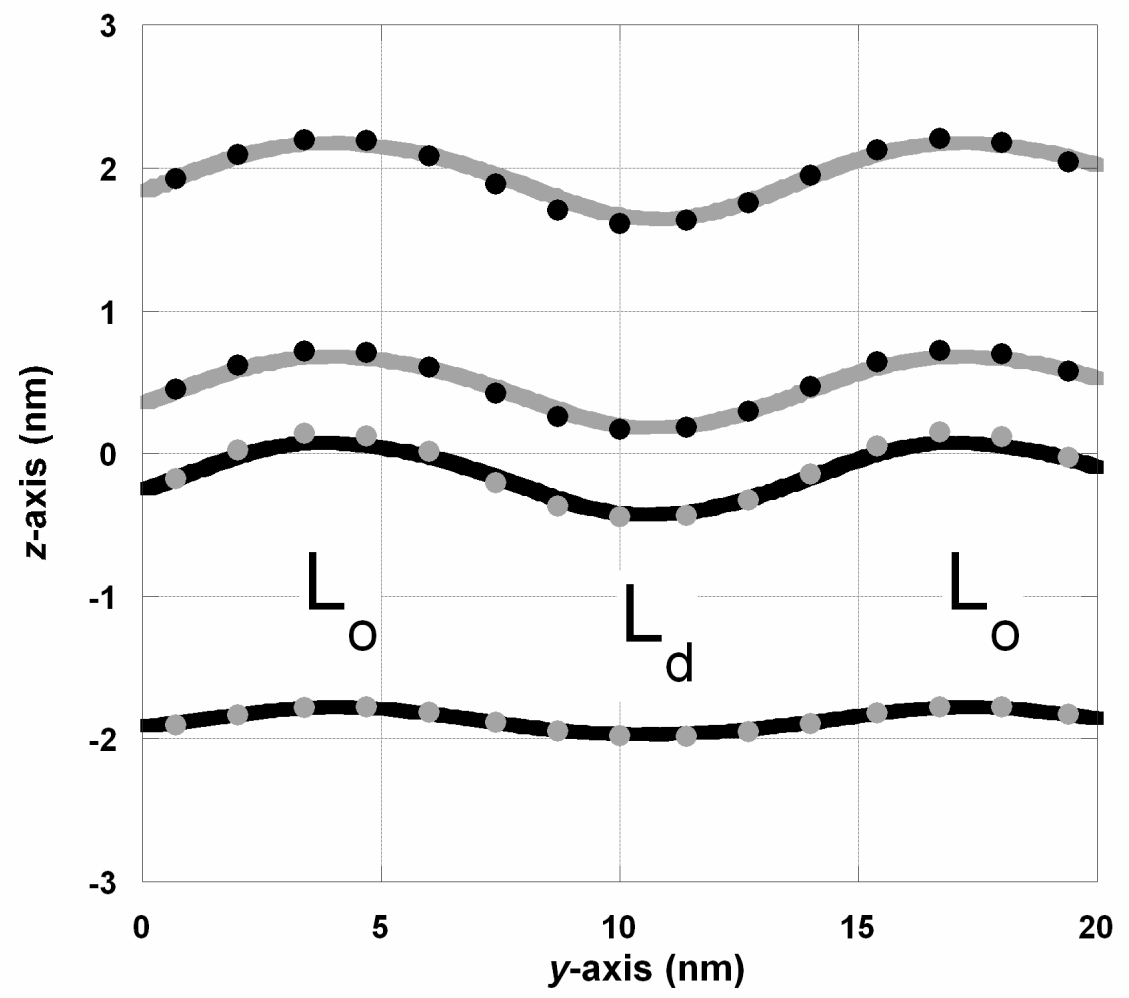

S12 – Positions of lipid backbone (solid), cholesterol hydroxyl (circle), and cholesterol tail (diamonds) for the top (gray) and bottom (black) leaflets in each simulation.

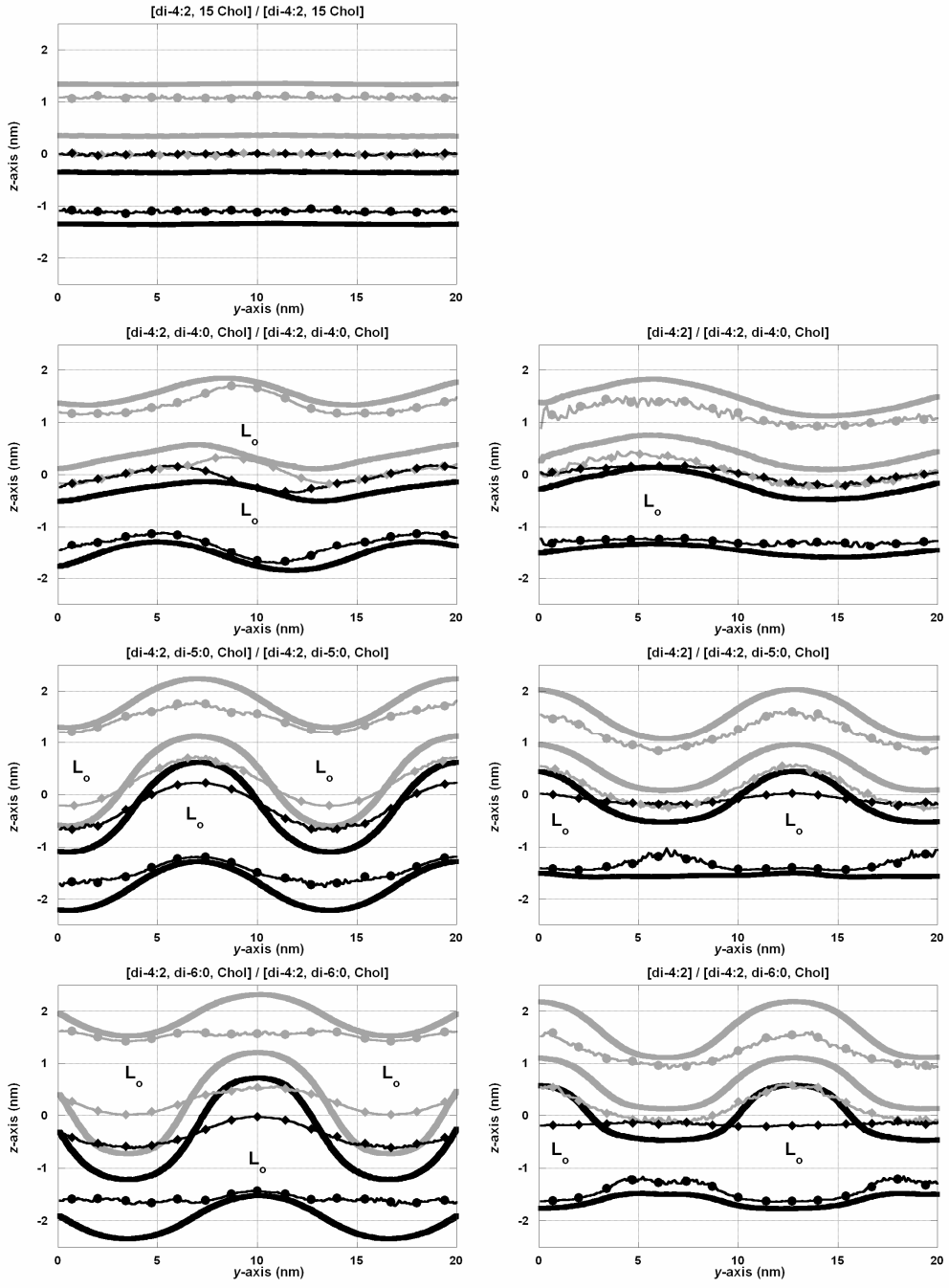

(1) Risselada, H. J.; Marrink, S. J. *Proc Natl Acad Sci U S A* **2008,** *105*, 17367-72
(2) Kiessling, V.; Crane, J. M.; Tamm, L. K. *Biophys J* **2006,** *91*, 3313-26
(3) Filippov, A.; Oradd, G.; Lindblom, G. *Biophys J* **2007,** *93*, 3182-90
(4) Kahya, N.; Scherfeld, D.; Bacia, K.; Poolman, B.; Schwille, P. *J Biol Chem* **2003,** *278*, 28109-15
(5) Chiantia, S.; Schwille, P.; Klymchenko, A. S.; London, E. *Biophys J* **2011,** *100*, L1-3